Waves Random Media **9** (1999) 441–457. Printed in the UK PII: S0959-7174(99)95309-0

An improved operator expansion algorithm for direct and inverse scattering computations

R Coifman†, M Goldberg‡, T Hrycak§, M Israeli‖ and V Rokhlin§

† Department of Mathematics, Yale University, New Haven, CT 06520, USA
‡ Physical Sciences Department, York College of Pennsylvania, York, PA 17405, USA
§ Department of Computer Science, Yale University, New Haven, CT 06520, USA
‖ Department of Computer Science, Technion, Haifa, Israel

Received 18 June 1998, in final form 9 February 1999

Abstract. In the first part of the paper we present an implementation of Milder's operator expansion formalism for acoustic scattering from a rough non-periodic surface. Our main contribution to the forward-field calculation is the development of two accurate ways of computing the order-zero normal differentiation operator N_0. The accuracy of our implementation is tested numerically. In the second part of our paper we apply this approach, combined with a continuation method, to an inverse scattering problem. The resulting scheme performs significantly better than the classical first-order methods.

1. Introduction

Scattering theory has been an active area of research for several decades. Several related problems belong to this field: acoustic and electromagnetic scattering form two large classes, which are further subdivided by assumptions on the underlying media and on the boundary conditions.

In direct problems one wants to calculate the field scattered by a given object. In two common situations, one knows either the values of the field on the scatterer (the Dirichlet problem), or the values of the normal derivative of the field on the boundary (the Neumann problem). Direct problems are usually well posed.

Inverse problems involve reconstructing the shape of a scatterer from the scattered field. These problems are ill posed: the solution has an unstable dependence on the input data.

For the convenience of the reader, we shall outline the progress made in acoustic scattering in a homogeneous medium from a sound-soft obstacle. A thorough discussion of this and related problems can be found in the references listed in the bibliography. The list of references is meant to be representative, rather than comprehensive.

The sound-soft scattering problem is characterized by the condition that the total field vanishes on the boundary of the scatterer. Thus, acoustic scattering is equivalent to the Dirichlet boundary value problem for the Helmholtz operator, with the scattered field equal to the negative of the known incident field. This problem is frequently solved by methods of potential theory. The single- and double-layer potentials relate a charge density on the boundary of the scatterer to the limiting values of the field and its normal derivative. The resulting integral equation is then solved in an appropriate function space, a common choice being the Lebesgue space L^2.

0959-7174/99/030441+17$19.50

If the boundary is sufficiently smooth (C^2, for example) the method of layer potentials falls within the scope of Fredholm theory, (see [3]). When the boundary is merely Lipschitz, the Dirichlet problem becomes much more difficult and was first studied for the Laplace operator, corresponding to a zero wavenumber. The boundedness of the double-layer potential as an operator on L^2 is a deep result in real-variable theory, proved in [1] for arbitrary Lipschitz constants (see also [2] for a survey of related topics). Invertibility of the double-layer potential in L^2 was first proved in [17], and extended to other L^p spaces in [6]. A thorough description of related research, together with an extensive bibliography, is given in [9]. Extensions to non-zero wavenumbers and higher dimensions are obtained and described in [7, 11, 14, 15], ([14] has an extensive bibliography).

For the direct problem, a straightforward numerical solution of the integral equations for the scattered field leads to an $O(n^3)$ algorithm.

For the inverse problem, numerical methods must cope with the problem's inherent ill posedness. Some commonly used approaches require that the scattered field can be analytically continued across the boundary of the scatterer, which makes the problem even more unstable. References [4, 10] contain detailed descriptions of these methods and discuss the difficulties associated with them.

In this paper, we consider both the direct and inverse problems of acoustic scattering in a homogeneous medium. Following Milder [12, 13], we start from the boundary integral equation formulation and expand the scattering amplitude in a series of readily computable terms. The principal tool in this formalism is the admittance operator relating the scattered field and its normal derivative at the scattering surface. See [18] for a thorough discussion of the operator expansion method and other issues in rough surface scattering.

We adapt Milder's theory to fast numerical evaluation of the field scattered from rough (Lipschitz) surfaces with compact support. Other authors, see [8], have already reported numerical implementations of Milder's theory. Our contribution, in the case of forward-scattering computations, is to implement N_0 (the order-zero normal differentiation operator) accurately, for the case of a compact boundary. We resolve the problems caused by the singularity of the symbol of N_0 as a pseudo-differential operator and that of the associated integral kernel. We also implement N_2. In two dimensions, the results of our implementations are compared with the exact solution obtained by classical integral-equation methods. We have validated our method numerically for boundaries with Lipschitz constant less than $\frac{1}{10}$. In the second part of the paper, we approximate N_s, the inversion-symmetric form of the admittance operator, by N_0 in the forward-field equation and invert the resulting expression to solve an inverse scattering problem in the far-field regime. We use a continuation method with respect to the frequency: at each step we apply Newton's method with the starting point given by the output from the previous step. Thus at each stage we create an approximation to the curve filtered at a higher frequency. Our method recovers some nonlinear effects not accounted for by the classical Fourier inversion method, and works well in some situations where the linear term approximation fails completely.

The paper is organized as follows. Section 2 introduces the notation used in the paper. Section 3 contains a detailed description of Milder's formalism, as well as the algebraic transformations to ensure that the relevant operators always act on functions of compact support. Then we describe two implementations of the operator N_0 and compare them. The section concludes with numerical results for the forward-field computations. We consider an inverse scattering problem in section 4 and discuss our continuation method for solving it. This section also includes some numerical experiments in surface reconstruction. We conclude with a summary in section 5.

2. Notation and definitions

We shall associate with the vector $X = (x_1, x_2, x_3) \in \mathbb{R}^3$, the vector $\bar{X} = (x_1, x_2, -x_3)$. x without subscripts will denote a vector in $\mathbb{R}^2$ and we shall sometimes write X as (x, x_3). Our scattering surface is denoted by Γ and is given by the graph of a compactly supported Lipschitz function $\zeta : \mathbb{R}^2 \to \mathbb{R}$. The points on the surface are thus of the form $(x, \zeta(x))$. The free-space Green's function $G(X, Y)$ for the wavenumber k is given by the formula

$$G(X, Y) = \frac{1}{4\pi} \frac{\exp[ik|X - Y|]}{|X - Y|} \tag{1}$$

for $X \neq Y$.

We shall frequently denote $G(X, Y)$ by $G_X(Y)$. We shall also use the following expression for G:

$$G((x, z), (x_0, z_0)) = g(|(x, z) - (x_0, z_0)|) \tag{2}$$

where $(x, z) \neq (x_0, z_0)$ and

$$g(r) = \frac{1}{4\pi} \frac{e^{ikr}}{r}. \tag{3}$$

Functions satisfying the Helmholtz equation will be called metaharmonic.

3. Computation of the scattered field

We consider the Dirichlet problem for acoustic scattering from a compactly supported perturbation of the plane. In subsection 3.1, we describe Milder's operator expansion formalism. We also discuss a modification we make to ensure that all integrations are performed over compact regions. The next two subsections (3.2 and 3.3) form the main part of our contribution to the forward-scattering computations: two implementations of the order-zero normal differentiation operator N_0. Because of the central role N_0 plays in the expansion formalism, we feel it is of interest to describe different ways of implementing it. In subsection 3.4, we compare the two methods. The last subsection (3.5) presents some numerical examples of computations of the scattered field.

3.1. The operator expansion formalism

The surface Γ of the scatterer is given by the graph of a compactly supported Lipschitz function $\zeta : \mathbb{R}^2 \to \mathbb{R}$. We consider the Dirichlet problem for the Helmholtz equation, i.e. we wish to solve

$$(\Delta + k^2)\Phi_{\text{scat}} = 0 \tag{4}$$

in the region lying above Γ, with the sound-soft boundary condition

$$\Phi_{\text{scat}}|_\Gamma = -\Phi_{\text{inc}}|_\Gamma \tag{5}$$

where Φ_{inc} is the (known) incoming wave and Φ_{scat} is the scattered wave.

Following Milder, see [12, 13], we begin with the Green–Helmholtz integral for the scattered field:

$$\Phi_{\text{scat}}(R) = \int_\Gamma \left(\frac{\partial G_R}{\partial n}(X)\Phi_{\text{scat}}(X) - \frac{\partial \Phi_{\text{scat}}}{\partial n}(X) G_R(X) \right) \mathrm{d}s(X) \tag{6}$$

where the free-space Green's function is defined by

$$G_R(X) = \frac{\exp[ik|X - R|]}{4\pi|X - R|}. \tag{7}$$

Milder has modified this formula to obtain

$$\Phi_{\text{scat}}(R) = 2\int_{\mathbb{R}^2} G_R(y, \zeta(y))(N_s\Phi_{\text{inc}})(y)\,\mathrm{d}y \tag{8}$$

where N_s has a formal operator power series expansion in ζ. Only even powers of ζ occur in the expansion, and N_s can be written as a series of operators

$$N_s = \sum_{j=0}^{\infty} N_{2j} = N_0 + N_2 + \cdots. \tag{9}$$

Already, the first two terms of this expansion provide an order-four approximation to the scattered potential, which surpasses the classical ones of Bragg or Kirchhoff (see [12]). The expressions for the operators N_0 and N_2 are given by the following formulae:

$$N_0 f = \left(\mathrm{i}\sqrt{k^2 - |\eta|^2}\,\hat{f}(\eta)\right)^{\vee} \tag{10}$$

$$N_2 f = -\tfrac{1}{2}N_0[\zeta, [\zeta, N_0]]N_0 f \tag{11}$$

where

$$[\zeta, N_0]g = \zeta(N_0 g) - N_0(\zeta g) \tag{12}$$

$\hat{f}$ is the Fourier transform and $\check{f}$ is the inverse Fourier transform of f.

Higher-order terms have simple expressions in terms of higher-order commutators, although their implementation gradually becomes more difficult.

Alternatively, N_0 can be viewed as a convolution operator with kernel $K(x, y)$ given by

$$K(x, y) = -2\frac{g'(|x - y|)}{|x - y|} \tag{13}$$

where

$$g(r) = \frac{1}{4\pi}\frac{\mathrm{e}^{\mathrm{i}kr}}{r}. \tag{14}$$

Note, that the kernel $K(x, y)$ is singular and is not a rapidly decaying function of $|x - y|$. Any accurate numerical implementation has to overcome these problems.

In our experiments the incident field originates at a point source located at S, so that

$$\Phi_{\text{inc}}(Y) = G_S(Y). \tag{15}$$

We calculate the scattered field $\Phi_{\text{scat}}(R)$ using N_0 or $N_0 + N_2$ instead of N_s. The resulting approximations are correct through second and fourth order in ζ, respectively. However, one cannot use formula (8) directly, since the functions $N_0\Phi_{\text{inc}}$, $(N_0 + N_2)\Phi_{\text{inc}}$ and $G_R(y, \zeta(y))$ are supported on the whole plane. Therefore, we modify formula (8) so that all non-local operators are applied to compactly supported functions and the final integration is performed on a compact set. First, since $G_{\bar{S}}(y)$ is metaharmonic above the boundary, (8) applied to $G_{\bar{S}}(y)$ gives:

$$G_{\bar{S}}(R) = -2\int G_R(y, \zeta(y))N_s G_{\bar{S}}(y)\,\mathrm{d}y \tag{16}$$

where $\bar{S}$ is the reflection of S across the XY-plane. Combining (15), (16) with (8), we obtain

$$\Phi_{\text{scat}}(R) = -G_{\bar{S}}(R) + 2\int G_R(y, \zeta(y))N_s(G_S - G_{\bar{S}})(y)\,\mathrm{d}y. \tag{17}$$

Note that the difference $G_S - G_{\bar{S}}$ vanishes outside the support of ζ.

Even though $G_S - G_{\bar{S}}$ is compactly supported, $N_s(G_S - G_{\bar{S}})$, in general, is not. We shall now describe the additional modifications that are made to (17) after N_s is replaced by N_0, to ensure integration over a compact set. Defining

$$\Phi^0_{\text{scat}}(R) = -G_{\bar{S}}(R) + 2\int G_R(y, \zeta(y))N_0(G_S - G_{\bar{S}})(y)\,\mathrm{d}y \tag{18}$$

we have

$$\Phi^0_{\text{scat}}(R) = -G_{\bar{S}}(R) + 2\int G_R(y, 0)N_0(G_S - G_{\bar{S}})(y)\,\mathrm{d}y$$
$$+2\int (G_R(y, \zeta(y)) - G_R(y, 0))N_0(G_S - G_{\bar{S}})(y)\,\mathrm{d}y. \tag{19}$$

Since N_0 is a symmetric operator, and

$$N_0 G_R(y) = N_0 G_{\bar{R}}(y) = \frac{\partial G_{\bar{R}}}{\partial y_3}(y, 0) \tag{20}$$

we immediately obtain

$$\Phi^0_{\text{scat}}(R) = -G_{\bar{S}}(R) + 2\int \frac{\partial G_{\bar{R}}}{\partial y_3}(y, 0)(G_S - G_{\bar{S}})(y)\,\mathrm{d}y$$
$$+2\int (G_R(y, \zeta(y)) - G_R(y, 0))N_0(G_S - G_{\bar{S}})(y)\,\mathrm{d}y. \tag{21}$$

Since both $G_R(y, \zeta(y)) - G_R(y, 0)$ and $\partial G_{\bar{R}}/\partial y_3$ are compactly supported, we see that the evaluation of $\Phi^0_{\text{scat}}(R)$ can be reduced to evaluation of inner products of the form $\langle N_0 f, g\rangle = \int N_0 f(y)g(y)\,\mathrm{d}y$, where both f and g are compactly supported.

The operator N_2 requires several similar decompositions starting from (17). We omit the details.

3.2. Implementation of the operator N_0

As shown in the previous subsection, computation of the approximate scattered field can be reduced to evaluation of inner products of the form $\langle N_0 f, g\rangle$, where both f and g are compactly supported.

A straightforward numerical implementation of N_0 would consist of approximating the Fourier integral by a DFT, multiplying by the symbol of N_0, and then applying an approximate inverse Fourier transform via another DFT. However, the symbol of N_0 as a pseudo-differential operator, $\mathrm{i}\sqrt{k^2 - |\eta^2|}$, is not differentiable on the circle $|\eta| = k$. Therefore, this direct approach would result in a low-order integration scheme and require a very fine uniform discretization in frequency to give accurate results.

In this subsection, we demonstrate one way of resolving this problem. Our approach can be applied to compute other Fourier integral operators with singular kernels. In our numerical experiments, we approximate Lipschitz curves and surfaces by smooth functions. Thus the function f (and g) is smooth in addition to being compactly supported. Therefore, the function $\hat{f}$ is numerically compactly supported and integrations involving products of $\hat{f}$ are effectively on compact subsets of the frequency space.

Our method of computing $\langle N_0 f, g\rangle$ involves expressing N_0 as a sum of two operators, T_1 and T_2, with the following properties:

- the symbol of T_1 is continuously differentiable to a prescribed order, and
- T_2 is a convolution with a smooth function.

We evaluate T_1 using the FFT on the frequency side. Since the symbol of T_1 is several times differentiable, it can be sampled relatively coarsely and still yield a good approximation.

The convolution with the smooth kernel of T_2 can be implemented efficiently by an FFT, where this time the FFT is not viewed as a discretization of the continuous Fourier transform, as it was when evaluating T_1, but as an algebraic operation which diagonalizes the discrete convolution. $\langle N_0 f, g\rangle$ is then evaluated by integration over the compact support of g.

We shall exhibit the decomposition of N_0 in three dimensions, the result being valid in two dimensions with only minor modifications.

We note (see [13]), that

$$N_0 f(x) = \frac{1}{(2\pi)^2}\int_{\mathbb{R}^2} \mathrm{i}q(\eta)\mathrm{e}^{\mathrm{i}x\cdot\eta}\hat{f}(\eta)\,\mathrm{d}\eta \tag{22}$$

where $q(\eta) = \sqrt{k^2 - |\eta|^2}$ is chosen to have a positive imaginary part when $|\eta|^2 > k^2$.

We fix a positive integer m and a positive real x_3. We decompose $N_0 f$ into two terms:

$$\begin{aligned} N_0 f(x) &= T_1 f(x) + T_2 f(x) \\ &= \frac{1}{(2\pi)^2}\int_{\mathbb{R}^2} \mathrm{i}q(\eta)[1-\mathrm{e}^{\mathrm{i}q(\eta)x_3}]^m \mathrm{e}^{\mathrm{i}x\cdot\eta}\hat{f}(\eta)\,\mathrm{d}\eta \\ &\quad + \frac{1}{(2\pi)^2}\int_{\mathbb{R}^2} \mathrm{i}q(\eta)\{1-[1-\mathrm{e}^{\mathrm{i}q(\eta)x_3}]^m\}\mathrm{e}^{\mathrm{i}x\cdot\eta}\hat{f}(\eta)\,\mathrm{d}\eta. \end{aligned} \tag{23}$$

Let us first look at T_1. Its symbol, $\sigma(T_1)$, is given by

$$\begin{aligned} \sigma(T_1) &= \mathrm{i}q(\eta)[1-\mathrm{e}^{\mathrm{i}q(\eta)x_3}]^m \\ &= \mathrm{i}q(\eta)\left[-\mathrm{i}q(\eta)x_3 + \frac{q^2(\eta){x_3}^2}{2} + \ldots\right]^m \\ &= c_1 q^{m+1}(\eta) + c_2 q^{m+2}(\eta) + \ldots. \end{aligned} \tag{24}$$

If m is odd, then $m+1$ is even, and $q^{m+1}(\eta)$ is a polynomial. Now, for $j = 1, 2$,

$$\frac{\mathrm{d}}{\mathrm{d}\eta_j} q(\eta) = \frac{\mathrm{d}}{\mathrm{d}\eta_j}\left(k^2 - |\eta|^2\right)^{1/2} = \frac{c\eta_j}{q(\eta)} \tag{25}$$

and

$$\frac{\mathrm{d}}{\mathrm{d}\eta_j} q^l(\eta) = c q^{l-2}(\eta)\eta_j. \tag{26}$$

Thus, each derivative in η reduces the exponent of q by two. If $l = 2j+1$, then $q^l(\eta)$ is j times continuously differentiable. In the above, if $m = 2n+1$, $m+2 = 2(n+1)+1$, then $\sigma(T_1)$, the symbol of T_1, is $n+1$ times continuously differentiable.

As for the operator T_2, we write

$$T_2(f)(x) = \int_{\mathbb{R}^2} K(x-y) f(y)\,\mathrm{d}y. \tag{27}$$

One can show that

$$K(x) = \sum_{n=1}^{m} (-1)^{n+1}\binom{m}{n} h(k, x, nx_3) \tag{28}$$

where

$$\begin{aligned} h(k, x, x_3) = -2\frac{\exp[\mathrm{i}k\sqrt{x^2+x_3^2}]}{4\pi\sqrt{x^2+x_3^2}}\Big\{ &\mathrm{i}k(x^2+x_3^2)^{-1/2} - (k^2x_3^2+1)(x^2+x_3^2)^{-1} \\ &-3\mathrm{i}kx_3^2(x^2+x_3^2)^{-3/2} + 3x_3^2(x^2+x_3^2)^{-2}\Big\}. \end{aligned} \tag{29}$$

Moreover, $h(k, x, x_3)$ is a smooth function of x for a positive x_3, and thus $K(x)$ is also smooth. Details of the derivation are given in the appendix.

3.3. An alternative implementation of the operator N_0

There is an alternative way of implementing the operator N_0. We can regard N_0 as a convolution with an integral kernel, which has a singularity at zero. This section sketches the details of this approach. The interested reader may see [16] for a thorough discussion of the relevant issues. In the following we derive an explicit expression for the kernel.

The Green's function for the upper half-space $G_{\{z>0\}}$ can be expressed in terms of the free-space Green's function G as follows,

$$G_{\{z>0\}}((x, z), (x_0, z_0)) = G((x, z), (x_0, z_0)) - G((x, -z), (x_0, z_0)). \tag{30}$$

The Poisson kernel p for the upper half-space is the outward normal derivative of the Green's function

$$\begin{aligned} p(x, (x_0, z_0)) &= -\frac{\partial}{\partial z} G_{\{z>0\}}((x, z), (x_0, z_0))\Big|_{z=0} \\ &= 2g'(|(x, 0) - (x_0, z_0)|)\frac{z_0}{|(x, 0) - (x_0, z_0)|}. \end{aligned} \tag{31}$$

The Dirichlet-to-Neumann operator N_0 can be expressed by the formula

$$N_0 f(x) = \lim_{z\to 0} -\frac{\partial}{\partial z}\int_{\mathbb{R}^2} p(y, (x, z)) f(y)\,\mathrm{d}y. \tag{32}$$

The kernel $K(x, y)$ of the Dirichlet-to-Neumann operator N_0, for $x \neq y$, is therefore the outward normal derivative of the Poisson kernel p (see also [18]),

$$K(x, y) = -\frac{\partial}{\partial z} p(y, (x, z))\Big|_{z=0} = -2\frac{g'(|x - y|)}{|x - y|}. \tag{33}$$

The operator N_0 has been implemented via the following approximation

$$\begin{aligned} N_0 f(x) \approx{}& \text{Trapezoidal sum for } \int K(x, y) f(y)\,\mathrm{d}y \\ &+ c_1 f(x) h^{-1} + c_2 \Delta f(x) h + c_3 f(x) k^2 h + \mathrm{O}(h^3) \end{aligned} \tag{34}$$

where Δ is the Laplace operator in $\mathbb{R}^2$ and h is the side-length of an elementary grid square. The constants c_1, c_2, c_3 can be computed numerically from the formula (34) using Richardson extrapolation, see [5], p 269.

A similar approach applies to the two-dimensional case. The free-space Green's function is then given by the formula

$$\rho(r) = \frac{\mathrm{i}}{4} H_0(kr) \tag{35}$$

and the kernel of N_0 is equal to

$$K(x, y) = -2\frac{\rho'(r)}{r} = \frac{\mathrm{i}k}{2}\frac{H_1(k|x - y|)}{|x - y|}. \tag{36}$$

We use the following approximation:

$$N_0 f(x) \approx \text{Trapezoidal sum for the } \int K(x, y) f(y)\,\mathrm{d}y + a_1(h) f(x) + a_2(h) f''(x) \tag{37}$$

where

$$a_1(h) = -\frac{\pi}{3h} - \frac{1}{2\pi}\left(E - \frac{1}{2} + \log\left(\frac{hk}{4\pi}\right)\right)hk^2 - \frac{\zeta(3)}{4\cdot(2\pi)^3}h^3k^4 + \frac{\mathrm{i}}{4}hk^2$$
$$a_2(h) = \frac{h}{2\pi} + \frac{\zeta(3)}{(2\pi)^3}h^3k^2 \tag{38}$$

and $E = 0.577\,215\ldots$ is the Euler constant.

3.4. Comparison of the two methods

We have described two different methods of implementing N_0. The first one, expressing N_0 as a sum of T_1 and T_2, seems to be rather general and may prove useful for other integral operators. The main idea is that a non-decaying, singular symbol is broken into two parts: the first is non-decaying but smooth, while the second is singular but rapidly decaying at infinity. The first part can be applied on the frequency side with a relatively coarse discretization to functions with a fast decaying Fourier transform. Thus we can accurately evaluate $T_1 f$ when f is smooth. The second symbol is not applied on the frequency side, but as a convolution operator on the space side. Since this symbol is rapidly decaying, the convolution kernel is smooth and, again, a relatively coarse discretization can be used. Thus we can accurately evaluate $T_2 f$ when f is compactly supported.

The second method of implementing N_0 illustrates how to calculate a convolution with a kernel having a singularity at 0 numerically. The method is more direct, but the correction coefficients have to be computed for each particular kernel.

3.5. Numerical results

In this subsection we present examples of numerical computations of approximate scattered fields. We report our results in two dimensions and compare them with the accurate values obtained using the classical integral-equation approach. We used the two-dimensional version of formula (18) to calculate $\Phi^0_{\mathrm{scat}}(R)$, and a similar expression when N_s is replaced by $N_0 + N_2$. The results have been obtained with N_0 implemented by the method described in section 3.3, after verifying that both methods give nearly identical results in test cases.

The integral-equation method requires, however, that the scatterer be bounded. When the scatterer is defined by a non-negative, compactly supported function ζ, it is possible to reduce the Dirichlet problem on the open domain above ζ to the Dirichlet problem for the exterior of a bounded region. To this end, we first construct a solution u to the Dirichlet problem for the upper half-space. The boundary values of u should match the given data away from the support of the curve and can be chosen arbitrarily on the support. Next we consider the lens-shaped region formed by reflecting ζ about the plane $z = 0$, and the antisymmetric Dirichlet boundary conditions given as follows: the boundary values on the upper half of the region are equal to the original ones minus the values of u on the curve, while the boundary values on the lower half are the negatives of the corresponding values on the upper half. We now solve the Dirichlet problem for the resulting symmetric domain with antisymmetric boundary values. Note that the solution vanishes everywhere on the plane $z = 0$ outside the bounded region. The sum of u and the solution for the symmetric region is the solution to the original problem.

Tables 1–3 present results of numerical simulations for a simple test curve. In all cases, the relative errors are computed for the reduced potential $\Phi = \Phi_{\mathrm{scat}} + G_{\tilde{S}}(R)$. Using the full potential, the relative errors are much smaller, but less meaningful. The errors are computed

Table 1. Relative error of the reduced potential with $N_s \approx N_0$.

	Height				
Wavenumber	1	0.5	0.25	0.125	0.0625
π	6.72×10^{-1}	1.74×10^{-1}	4.77×10^{-2}	1.27×10^{-2}	3.27×10^{-3}
2π	8.10×10^{-1}	3.24×10^{-1}	8.56×10^{-2}	2.20×10^{-2}	5.60×10^{-3}
4π	9.52×10^{-1}	3.92×10^{-1}	7.74×10^{-2}	1.85×10^{-2}	4.66×10^{-3}
8π	1.13×10^{0}	5.19×10^{-1}	9.43×10^{-2}	2.16×10^{-2}	5.05×10^{-3}
16π	1.24×10^{0}	4.82×10^{-1}	8.64×10^{-2}	2.21×10^{-2}	5.37×10^{-3}
32π	1.30×10^{0}	5.68×10^{-1}	8.34×10^{-2}	2.06×10^{-2}	5.49×10^{-3}

Table 2. Relative error of the reduced potential with $N_s \approx N_0 + N_2$.

	Height				
Wavenumber	1	0.5	0.25	0.125	0.0625
π	2.82×10^{-1}	2.21×10^{-2}	1.84×10^{-3}	1.34×10^{-4}	2.44×10^{-5}
2π	3.81×10^{-1}	2.10×10^{-2}	1.76×10^{-3}	1.25×10^{-4}	3.28×10^{-5}
4π	1.06×10^{0}	9.09×10^{-2}	5.67×10^{-3}	3.72×10^{-4}	5.32×10^{-5}
8π	7.81×10^{-1}	2.21×10^{-1}	9.81×10^{-3}	4.18×10^{-4}	7.59×10^{-5}
16π	1.04×10^{0}	3.64×10^{-1}	9.18×10^{-3}	4.47×10^{-4}	2.15×10^{-4}
32π	1.12×10^{0}	5.22×10^{-1}	7.98×10^{-3}	5.09×10^{-4}	6.76×10^{-4}

Table 3. Relative difference of the reduced potentials with $N_s \approx N_0$ and $N_s \approx N_0 + N_2$.

	Height				
Wavenumber	1	0.5	0.25	0.125	0.0625
π	8.59×10^{-1}	1.95×10^{-1}	4.94×10^{-2}	1.28×10^{-2}	3.28×10^{-3}
2π	8.68×10^{-1}	3.38×10^{-1}	8.69×10^{-2}	2.21×10^{-2}	5.62×10^{-3}
4π	9.86×10^{-1}	4.52×10^{-1}	8.21×10^{-2}	1.88×10^{-2}	4.68×10^{-3}
8π	1.03×10^{0}	5.80×10^{-1}	1.03×10^{-1}	2.20×10^{-2}	5.07×10^{-3}
16π	9.81×10^{-1}	6.54×10^{-1}	9.42×10^{-2}	2.25×10^{-2}	5.39×10^{-3}
32π	1.02×10^{0}	7.70×10^{-1}	9.04×10^{-2}	2.09×10^{-2}	5.48×10^{-3}

in the l^2 norm:

$$E = \frac{\left(\sum_i |\Phi_i - \tilde{\Phi}_i|^2\right)^{1/2}}{\left(\sum_i |\tilde{\Phi}_i|^2\right)^{1/2}} \tag{39}$$

where Φ_i is the reduced potential at the ith receiver obtained by the algorithm and $\tilde{\Phi}_i$ is the corresponding value obtained by solving the combined field integral equations directly (see [4], p 67, for a thorough description).

Note how the relative errors increase with the height of the curve, but that they remain nearly constant at a fixed height as the wavenumber increases.

Table 4 records the result of a scattering experiment performed for a curve having only low-frequency components. The objective was to determine the dependence of the term N_2 on the wavenumber of the incident field. We find that the error depends only weakly on the wavenumber of the incident field once it exceeds the highest frequency of the curve.

Table 4. Relative difference of the reduced potentials with $N_s \approx N_0$ and $N_s \approx N_0 + N_2$ for a smooth curve.

	Height					
Wavenumber	0.25	0.125	0.0625	0.031 25	0.015 625	0.007 8125
π	1.17×10^{-1}	3.08×10^{-2}	8.07×10^{-3}	2.07×10^{-3}	5.26×10^{-4}	1.33×10^{-4}
2π	1.67×10^{-1}	3.97×10^{-2}	1.01×10^{-2}	2.58×10^{-3}	6.52×10^{-4}	1.64×10^{-4}
4π	2.12×10^{-1}	3.50×10^{-2}	7.75×10^{-3}	1.88×10^{-3}	4.64×10^{-4}	1.16×10^{-4}
8π	2.43×10^{-1}	4.14×10^{-2}	7.74×10^{-3}	1.76×10^{-3}	4.31×10^{-4}	1.07×10^{-4}
16π	2.13×10^{-1}	4.65×10^{-2}	9.95×10^{-3}	1.89×10^{-3}	4.31×10^{-4}	1.05×10^{-4}
32π	1.73×10^{-1}	4.16×10^{-2}	1.11×10^{-2}	2.47×10^{-3}	4.71×10^{-4}	1.07×10^{-4}
64π	1.67×10^{-1}	3.71×10^{-2}	9.96×10^{-3}	2.73×10^{-3}	6.15×10^{-4}	1.18×10^{-4}
128π	1.70×10^{-1}	3.61×10^{-2}	8.95×10^{-3}	2.47×10^{-3}	6.82×10^{-4}	1.54×10^{-4}
256π	1.68×10^{-1}	3.68×10^{-2}	8.74×10^{-3}	2.22×10^{-3}	6.15×10^{-4}	1.70×10^{-4}

4. Inverse scattering

We now turn to the problem of inverse scattering. We wish to study nonlinear interactions of the scatterer with itself in the problem of reconstructing a surface given its far field. Milder's formalism, with its order-by-order expansion in powers of ζ, provides a convenient framework for such analysis. One of our goals is to reconstruct a surface, for which the classical linear approach fails. Section 4.1 describes our experiment and methodology, while section 4.2 contains numerical examples.

4.1. Description of the experiment

Starting from formula (21), we first develop an expansion for Φ^0_{scat} in negative powers of the distance between receiver and scatterer.

We introduce some more notation. We shall write $X = r\alpha$, $S = r\sigma$, $R = r\omega$, where $|\alpha| = |\sigma| = |\omega| = 1$. As before, a bar will denote that the third coordinate has a negative sign, for example, if $\alpha = (\alpha_1, \alpha_2, \alpha_3)$, then $\bar{\alpha} = (\alpha_1, \alpha_2, -\alpha_3)$. Also, as before, for $Y \in \mathbb{R}^3$, and Y on the scattering boundary, we shall write $Y = (y, \zeta(y))$, where $y = (y_1, y_2) \in \mathbb{R}^2$. We denote the scalar product of vectors X and Y by $X \cdot Y$.

The formula (21) derived in section 3.1

$$\Phi^0_{\text{scat}}(R) = -G_{\bar{S}}(R) + 2\int \frac{\partial G_{\bar{R}}}{\partial y_3}(y,0)(G_S - G_{\bar{S}})(y)\,\mathrm{d}y$$
$$+2\int (G_R(y,\zeta(y)) - G_R(y,0))N_0(G_S - G_{\bar{S}})(y)\,\mathrm{d}y \tag{40}$$

gives rise to a far-field approximation. Assuming that $|Y| \ll |S| = r$, we have the following asymptotic expansions

$$|S - Y| = \sqrt{|S|^2 - 2Y\cdot S + |Y|^2} = r - \frac{Y\cdot S}{r} + \mathrm{O}\left(\frac{1}{r}\right) \tag{41}$$

$$|S - Y|^{-1} = \frac{1}{r} + \mathrm{O}\left(\frac{1}{r^2}\right) \tag{42}$$

$$G_S(Y) = \frac{\exp[\mathrm{i}k|S-Y|]}{4\pi|S-Y|} = \frac{\mathrm{e}^{\mathrm{i}kr}}{4\pi r}\exp[-\mathrm{i}kY\cdot S/r] + \mathrm{O}\left(\frac{1}{r^2}\right). \tag{43}$$

From (43) we find that

$$G_S(y,\zeta(y)) - G_{\bar{S}}(y,\zeta(y)) = -\mathrm{i}\frac{\mathrm{e}^{\mathrm{i}kr}}{2\pi r}\exp[-\mathrm{i}k(\sigma_1,\sigma_2)\cdot y]\sin(k\sigma_3\zeta(y)) + \mathrm{O}\left(\frac{1}{r^2}\right). \tag{44}$$

Similarly,

$$G_R(y,\zeta(y)) - G_R(y,0) = \frac{\mathrm{e}^{\mathrm{i}kr}}{4\pi r}\exp[-\mathrm{i}k(\omega_1,\omega_2)\cdot y]\left(\mathrm{e}^{-\mathrm{i}k\omega_3\zeta(y)} - 1\right) + \mathrm{O}\left(\frac{1}{r^2}\right). \tag{45}$$

Moreover,

$$G_{\bar{R}}(y,y_3) = \frac{\mathrm{e}^{\mathrm{i}kr}}{4\pi r}\exp[-\mathrm{i}k\bar{\omega}\cdot(y,y_3)] + \mathrm{O}\left(\frac{1}{r^2}\right) \tag{46}$$

and therefore

$$\frac{\partial G_{\bar{R}}}{\partial y_3}(y,0) = \mathrm{i}k\omega_3\frac{\mathrm{e}^{\mathrm{i}kr}}{4\pi r}\exp[-\mathrm{i}k(\omega_1,\omega_2)\cdot y] + \mathrm{O}\left(\frac{1}{r^2}\right). \tag{47}$$

Combining (44), (45), (47) with (40), we obtain

$$\begin{aligned}\Phi_{\mathrm{scat}}(R) \approx {} & -G_{\bar{S}}(R) + k\omega_3\frac{\mathrm{e}^{2\mathrm{i}kr}}{4\pi^2r^2}\int_{\mathbb{R}^2}\exp[-\mathrm{i}k(\omega_1+\sigma_1,\omega_2+\sigma_2)\cdot y]\sin(k\sigma_3\zeta)\,\mathrm{d}y \\ & -\mathrm{i}\frac{\mathrm{e}^{2\mathrm{i}kr}}{4\pi^2r^2}\int_{\mathbb{R}^2}\exp[-\mathrm{i}k(\omega_1,\omega_2)\cdot y]\left(\mathrm{e}^{-\mathrm{i}k\omega_3\zeta} - 1\right) \\ & \times N_0\left(\exp[-\mathrm{i}k(\sigma_1,\sigma_2)\cdot y]\sin(k\sigma_3\zeta)\right)\mathrm{d}y + \mathrm{O}\left(\frac{1}{r^3}\right).\end{aligned} \tag{48}$$

This leads to an expression in terms of the Fourier coefficients

$$\begin{aligned}\Phi_{\mathrm{scat}}(R) \approx {} & -G_{\bar{S}}(R) + k\omega_3\frac{\mathrm{e}^{2\mathrm{i}kr}}{4\pi^2r^2}\left[\sin(k\sigma_3\zeta)\right]^{\wedge}(k\omega_1 + k\sigma_1, k\omega_2 + k\sigma_2)) \\ & -\mathrm{i}\frac{\mathrm{e}^{2\mathrm{i}kr}}{4\pi^2r^2}\left[\left(\mathrm{e}^{-\mathrm{i}k\omega_3\zeta} - 1\right)N_0\left(\exp[-\mathrm{i}k(\sigma_1,\sigma_2)\cdot y]\sin(k\sigma_3\zeta)\right)\right]^{\wedge}(k\omega_1, k\omega_2) \\ & +\mathrm{O}\left(\frac{1}{r^3}\right).\end{aligned} \tag{49}$$

In the special case, when the source is directly above, this formula becomes

$$\begin{aligned}\Phi_{\mathrm{scat}}(R) \approx {} & -G_{\bar{S}}(R) + k\omega_3\frac{\mathrm{e}^{2\mathrm{i}kr}}{4\pi^2r^2}\left[\sin(k\zeta)\right]^{\wedge}(k\omega_1, k\omega_2) \\ & -\mathrm{i}\frac{\mathrm{e}^{2\mathrm{i}kr}}{4\pi^2r^2}\left[\left(\mathrm{e}^{-\mathrm{i}k\omega_3\zeta} - 1\right)N_0\left(\sin(k\zeta)\right)\right]^{\wedge}(k\omega_1, k\omega_2) + \mathrm{O}\left(\frac{1}{r^3}\right).\end{aligned} \tag{50}$$

Similarly, for the two-dimensional case, one can derive the following formula:

$$\begin{aligned}\Phi_{\mathrm{scat}}(R) \approx {} & -G_{\bar{S}}(R) + \mathrm{i}\omega_3\frac{\mathrm{e}^{2\mathrm{i}kr}}{2\pi r}\left[\sin(k\zeta)\right]^{\wedge}(k\omega_1) \\ & +\frac{\mathrm{e}^{2\mathrm{i}kr}}{2\pi kr}\left[\left(\mathrm{e}^{-\mathrm{i}k\omega_3\zeta} - 1\right)N_0\left(\sin(k\zeta)\right)\right]^{\wedge}(k\omega_1) + \mathrm{O}\left(\frac{1}{r^2}\right).\end{aligned} \tag{51}$$

Although we used expression (51) in our numerical experiments, we would like to mention the following formula because of its appealing simplicity. For small elevations $k\zeta$, the sines and the exponentials can be expanded in powers of their arguments, yielding

$$\Phi_{\mathrm{scat}}(R) \approx -G_{\bar{S}}(R) + \mathrm{i}k\omega_3\frac{\mathrm{e}^{2\mathrm{i}kr}}{2\pi r}\left(\zeta - \zeta N_0\zeta\right)^{\wedge}(k\omega_1) + \mathrm{O}\left(\frac{1}{r^2}\right). \tag{52}$$

A similar result holds in three dimensions.

Let us now describe the geometric setup in two dimensions. The function ζ is supported on the interval $[-1, 1]$. The receivers at which we measure the scattered field are located on a semicircle of radius 10^5 in such a way that their projections on the x-axis are equispaced. The number of receivers is $\lfloor 2k/\pi \rfloor$. The source is located at the point $(0, 10^5)$.

Our reconstruction of ζ proceeds as follows.

- **Step 0**. We set the initial approximation to zero.
- **Step 1**. We choose an initial value for the wavenumber k and seek an approximation to the function ζ by a trigonometric polynomial of degree not exceeding k. Substituting

$$\zeta = \sum_{n=-k}^{k} c_n e^{int} \tag{53}$$

  in (51), we solve for the coefficients c_n using Newton's method with the previous approximation as the starting point. The resulting solution represents the Fourier coefficients of ζ corresponding to the frequencies not exceeding k.
- **Step 2**. We increase k to a new value k' ($k' = 2k$ is a convenient choice). We repeat step 1 with the previous approximation to ζ as our starting point. More precisely, we approximate ζ by the Fourier series $\sum_{n=-k'}^{k'} c_n e^{int}$ and determine the coefficients c_n by solving (51) using Newton's method starting from the previous result:

$$c'_n = \begin{cases} c_n & \text{for } |n| \leqslant k \\ 0 & \text{for } |n| > k \end{cases} \tag{54}$$

  where the coefficients c_n come from step 1.

We now iterate step 1 and step 2 until we reach a prescribed frequency k_0. For a complete reconstruction we need to choose k_0 larger than the highest frequency of the curve.

We have observed experimentally that the continuation method described above converges for a larger class of surfaces than Newton's method starting at $\zeta = 0$.

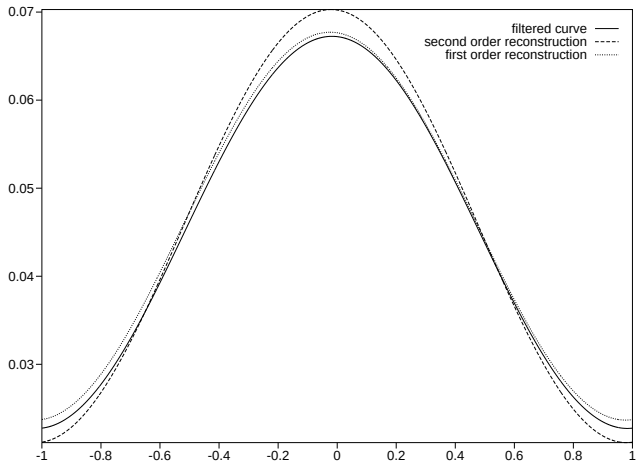

Figure 1. Reconstructions of the curve filtered at $k = \pi$. Filtered curve ——; second-order reconstruction - - - -; first-order reconstruction · · · · · ·.

4.2. Numerical results

Figures 1–6 illustrate the continuation method as described in the previous subsection. The solid curve in the final figure is the unknown curve to be reconstructed. The first figure shows a filtered version of that curve at wavenumber π, and the reconstruction carried out using Newton's method starting from the zero curve. The second-order reconstruction is plotted together with the 'classical' linear reconstruction. The output of the second-order reconstruction is then the starting point for the next stage, where the wavenumber doubles (and so does the number of receivers on the semicircle). We proceed successively, as outlined in section 4.1, until we reach the wavenumber that is above the highest frequency of the curve. At each stage we attempt to reconstruct the true curve filtered at the corresponding wavenumber. The final reconstruction using the second-order method with continuation approximates the

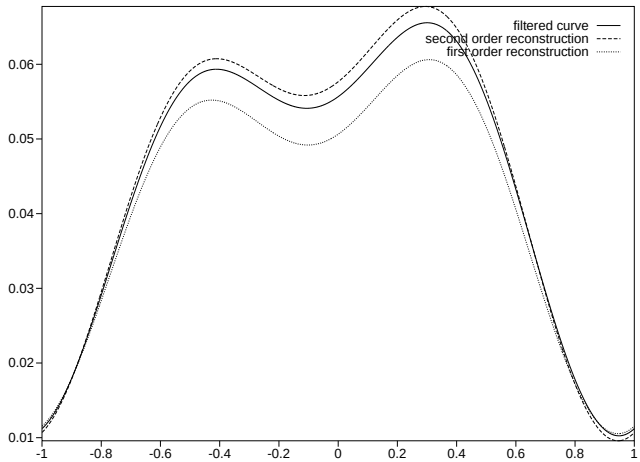

Figure 2. Reconstructions of the curve filtered at $k = 2\pi$. Filtered curve ——; second-order reconstruction - - - -; first-order reconstruction · · · · · ·.

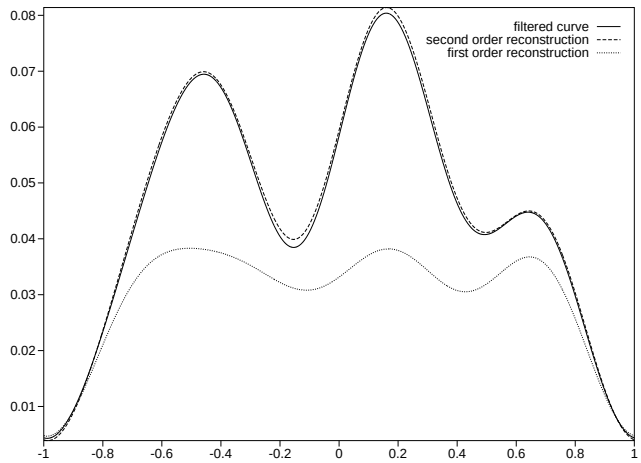

Figure 3. Reconstructions of the curve filtered at $k = 4\pi$. Filtered curve ——; second-order reconstruction - - - -; first-order reconstruction · · · · · ·.

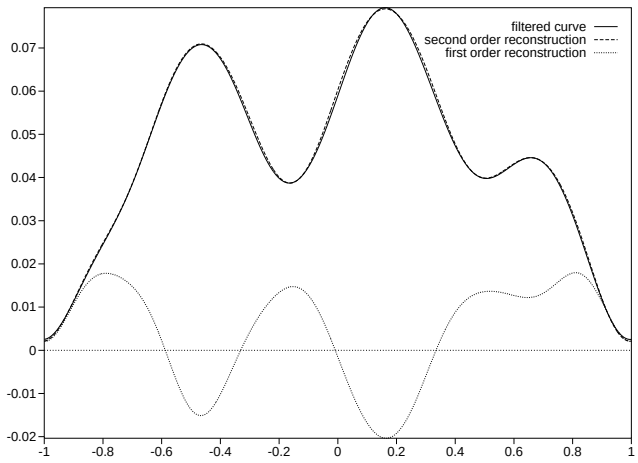

Figure 4. Reconstructions of the curve filtered at $k = 8\pi$. Filtered curve ——; second-order reconstruction - - - -; first-order reconstruction · · · · · ·.

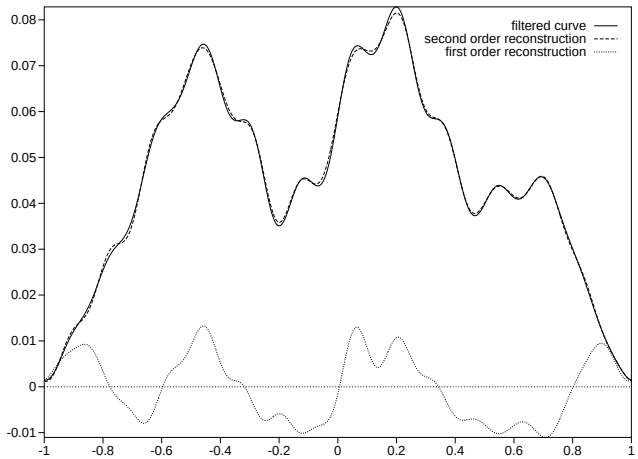

Figure 5. Reconstructions of the curve filtered at $k = 16\pi$. Filtered curve ——; second-order reconstruction - - - -; first-order reconstruction · · · · · ·.

curve very well. The first-order reconstruction is good for the first two stages but then moves further and further away from the actual curve.

5. Conclusions and summary

We present an implementation of Milder's operator expansion algorithm for acoustic scattering with Dirichlet boundary condition. We modify the integral used by Milder to ensure that all integral operators are applied to compactly supported functions and integrations are performed on bounded sets. Our main contribution to the forward-field calculation has been the development of two accurate ways of implementing the N_0 operator. We have also combined Milder's formalism together with a continuation method in frequency to reconstruct accurately rough boundaries with rather large heights. We have presented examples for which our

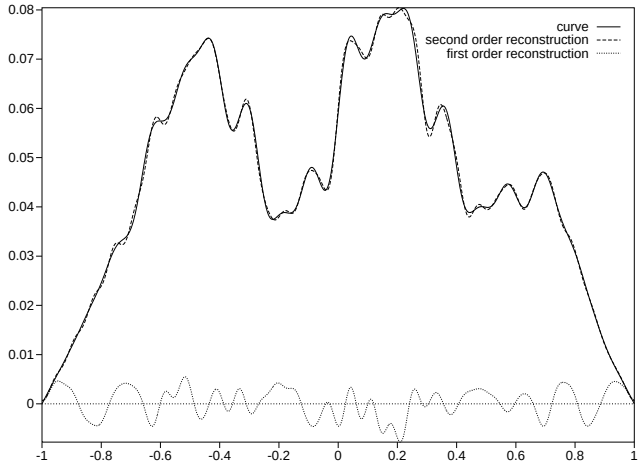

Figure 6. Reconstructions of the original curve with $k = 32\pi$. Original curve ——; second-order reconstruction - - - -; first-order reconstruction · · · · · ·.

method using second-order terms works, but for which the first-order reconstruction fails. Our numerical results suggest that the higher-order approximation errors from incident fields having higher wavenumber than the frequency content of the boundary tend to remain nearly constant as the wavenumber of the incident field increases.

A scheme for the fast evaluation of the Helmholtz potentials can be added to accelerate the algorithm. Such methods are currently being developed by several authors.

Acknowledgments

The authors would like to thank Christopher Hatchell for editing the manuscript and the referees for their many helpful suggestions. This research was supported by DARPA/AFOSR under Grant F49620-97-1-0011.

Appendix

In this appendix, we provide a detailed derivation of the kernel of the convolution operator T_2 defined in section 3.2.

From (23) we obtain

$$\begin{aligned} T_2(f)(x) &= \frac{1}{(2\pi)^2}\int_{\mathbb{R}^2}\int_{\mathbb{R}^2} \mathrm{i}q(\eta)\{1-[1-\mathrm{e}^{\mathrm{i}q(\eta)x_3}]^m\}\mathrm{e}^{-\mathrm{i}y\cdot\eta}\mathrm{e}^{\mathrm{i}x\cdot\eta} f(y)\,\mathrm{d}y\,\mathrm{d}\eta \\ &= \int_{\mathbb{R}^2} \mathrm{d}y f(y)\frac{1}{(2\pi)^2}\int_{\mathbb{R}^2} \mathrm{i}q(\eta)\{1-[1-\mathrm{e}^{\mathrm{i}q(\eta)x_3}]^m\}\mathrm{e}^{\mathrm{i}(x-y)\cdot\eta}\,\mathrm{d}\eta \\ &= \int_{\mathbb{R}^2} K(x-y)f(y)\,\mathrm{d}y \end{aligned} \tag{55}$$

where

$$\begin{aligned} K(x) &= \frac{1}{(2\pi)^2}\int_{\mathbb{R}^2} \mathrm{i}q(\eta)\{1-[1-\mathrm{e}^{\mathrm{i}q(\eta)x_3}]^m\}\mathrm{e}^{\mathrm{i}x\cdot\eta}\,\mathrm{d}\eta \\ &= \frac{1}{(2\pi)^2}\int_{\mathbb{R}^2} \mathrm{i}q(\eta)\sum_{n=1}^{m}(-1)^{n+1}\binom{m}{n}\mathrm{e}^{\mathrm{i}q(\eta)nx_3}\mathrm{e}^{\mathrm{i}x\cdot\eta}\,\mathrm{d}\eta \end{aligned}$$

$$= \sum_{n=1}^{m} (-1)^{n+1} \binom{m}{n} h(k, x, nx_3) \tag{56}$$

with

$$h(k, x, x_3) \equiv \frac{1}{(2\pi)^2} \int_{\mathbb{R}^2} \mathrm{i} q(\eta) \mathrm{e}^{\mathrm{i} x \cdot \eta} \mathrm{e}^{\mathrm{i} q(\eta) x_3} \, \mathrm{d}\eta. \tag{57}$$

We note that $h(k, x, x_3)$ can also be expressed as

$$h(k, x, x_3) = \frac{-\mathrm{i}}{(2\pi)^2} \frac{\partial^2}{\partial {x_3}^2} \int_{\mathbb{R}^2} \mathrm{e}^{\mathrm{i} x \cdot \eta} \mathrm{e}^{\mathrm{i} q(\eta) x_3} \frac{\mathrm{d}\eta}{q(\eta)}. \tag{58}$$

We shall use the spectral form of the free-space Green's function, see [13],

$$\frac{\exp[\mathrm{i} k ||X - Y||]}{4\pi ||X - Y||} = \frac{\mathrm{i}}{2} \frac{1}{(2\pi)^2} \int_{\mathbb{R}^2} \exp[\mathrm{i}(x - y) \cdot \eta + \mathrm{i} q(\eta) |x_3 - y_3|] \frac{\mathrm{d}\eta}{q(\eta)}. \tag{59}$$

Again, since x_3 is positive, setting $Y = 0$, we obtain

$$\frac{\exp[\mathrm{i} k \sqrt{x^2 + x_3^2}]}{4\pi \sqrt{x^2 + x_3^2}} = \frac{\mathrm{i}}{2} \frac{1}{(2\pi)^2} \int_{\mathbb{R}^2} \exp[\mathrm{i} x \cdot \eta + \mathrm{i} q(\eta) x_3] \frac{\mathrm{d}\eta}{q(\eta)} \tag{60}$$

where $x^2 = x_1^2 + x_2^2$. Substitution of (60) into (58) gives

$$h(k, x, x_3) = -2 \frac{\partial^2}{\partial x_3^2} \left(\frac{\exp[\mathrm{i} k \sqrt{x^2 + x_3^2}]}{4\pi \sqrt{x^2 + x_3^2}} \right). \tag{61}$$

After a straightforward calculation, we obtain:

$$h(k, x, x_3) = -2 \, \frac{\exp[\mathrm{i} k \sqrt{x^2 + x_3^2}]}{4\pi \sqrt{x^2 + x_3^2}} \Big\{ \mathrm{i} k (x^2 + x_3^2)^{-1/2} - (k^2 x_3^2 + 1)(x^2 + x_3^2)^{-1}$$
$$-3\mathrm{i} k x_3^2 (x^2 + x_3^2)^{-3/2} + 3 x_3^2 (x^2 + x_3^2)^{-2} \Big\}. \tag{62}$$

References

[1] Coifman R R, McIntosh A and Meyer Y 1982 L'intégrale de Cauchy définit un operateur borné sur L^2 pour les courbes Lipschitziennes *Ann. Math.* **116** 361–87 (in French)

[2] Coifman R R and Meyer Y 1986 *Nonlinear Harmonic Analysis, Operator Theory, and PDE (Ann. Math. Stud. 112)* (Princeton, NJ: Princeton University Press)

[3] Colton D and Kress R 1983 *Integral Equation Methods in Scattering Theory* (New York *et al* : Wiley)

[4] Colton D and Kress R 1998 *Inverse Acoustic and Electromagnetic Scattering Theory* 2nd edn (New York: Springer)

[5] Dahlquist G and Björck A 1974 *Numerical Methods* (Englewood Cliffs, NJ: Prentice-Hall)

[6] Dahlberg B and Kenig C 1987 Hardy spaces and the Neumann problem in L^p for Laplace's equation in Lipschitz domains *Ann. Math.* **125** 437–66

[7] Jaweth B and Mitrea M 1995 Higher-dimensional electromagnetic scattering theory on C^1 and Lipschitz domains *Am. J. Math.* **117** 929–63

[8] Kaczkowski P J and Thorsos E I 1994 Application of the operator expansion method to scattering from one-dimensional moderately rough Dirichlet random surfaces *J. Acoust. Soc. Am.* **96** 957–72

[9] Kenig C E 1994 *Harmonic Analysis Techniques for Second-Order Elliptic Boundary Value Problems (CBMS Regional Conference Series in Mathematics 83 (St Louis, 1991))* (Providence, RI: American Mathematical Society)

[10] Kirsch A 1996 *An Introduction to the Mathematical Theory of Inverse Problems* (New York: Springer)

[11] McIntosh A and Mitrea M 1996 Clifford algebras and Maxwell's equations in Lipschitz domains *Macquairie Mathematics Reports* No. 96/210
[12] Milder D M 1991 An improved formalism for wave scattering from rough surfaces *J. Acoust. Soc. Am.* **89** 529–41
[13] Milder D M 1996 Role of the admittance operator in rough-surface scattering *J. Acoust. Soc. Am.* **100** 759–68
[14] Mitrea D, Mitrea M and Pipher J 1997 Vector potential theory on non-smooth domains in $\mathbb{R}^3$ and applications to electromagnetic scattering *J. Fourier Anal. Appl.* **3** 131–92
[15] Mitrea M 1995 The method of layer potentials in electromagnetic scattering theory on non-smooth domains *Duke Math. J.* **77** 111–33
[16] Sidi A and Israeli M 1988 Quadrature methods for periodic singular and weakly singular Fredholm integral equations *J. Sci. Comput.* **3** 201–31
[17] Verchota G 1984 Layer potentials and regularity for the Dirichlet problem for Laplace's equation *J. Funct. Anal.* **59** 572–611
[18] Voronovich A G 1999 *Wave Scattering from Rough Surfaces* 2nd edn (New York: Springer)